

PIP-Net: Pedestrian Intention Prediction in the Wild

Mohsen Azarmi ^{*}, Mahdi Rezaei ^{*}, He Wang [†], Sebastien Glaser [‡]

^{*}Institute for Transport Studies, University of Leeds, United Kingdom

[†]Department of Computer Science, University College London, United Kingdom

[‡]Centre for Accident Research and Road Safety, Queensland University of Technology, Australia

Abstract—Accurate pedestrian intention prediction (PIP) by Autonomous Vehicles (AVs) is one of the current research challenges in this field. In this article, we introduce PIP-Net, a novel framework designed to predict pedestrian crossing intentions by AVs in real-world urban scenarios. We offer two variants of PIP-Net designed for different camera mounts and setups. Leveraging both kinematic data and spatial features from the driving scene, the proposed model employs a recurrent and temporal attention-based solution, outperforming state-of-the-art performance. To enhance the visual representation of road users and their proximity to the ego vehicle, we introduce a categorical depth feature map, combined with a local motion flow feature, providing rich insights into the scene dynamics. Additionally, we explore the impact of expanding the camera’s field of view, from one to three cameras surrounding the ego vehicle, leading to enhancement in the model’s contextual perception. Depending on the traffic scenario and road environment, the model excels in predicting pedestrian crossing intentions up to 4 seconds in advance which is a breakthrough in current research studies in pedestrian intention prediction. Finally, for the first time, we present the Urban-PIP dataset, a customised pedestrian intention prediction dataset, with multi-camera annotations in real-world automated driving scenarios.

Index Terms—Autonomous vehicles, pedestrian crossing behaviour, pedestrian intention prediction, computer vision, deep neural networks.

I. INTRODUCTION

PEDESTRIANS are the most vulnerable road users and face a high risk of fatal accidents [1]. Ensuring pedestrian safety in automated driving, particularly in mixed AV-pedestrian traffic scenarios, heavily relies on the AV’s capability in “pedestrian intention prediction (PIP)” [2]. A PIP system determines if a pedestrian is likely to cross the road shortly (within the next few seconds). This study aims to investigate the critical visual clues that pedestrians exhibit when they intend to cross the road, and then provide a model which predicts crossing behaviour a few seconds in advance.

Anticipating pedestrian crossing behaviour is a difficult task due to various environmental factors that affect human intention [3], [4]. Even in the simulated scenarios in which the majority of parameters are under control, crossing prediction is a challenging endeavour [5]. Factors like interactions with other pedestrians, traffic signs, road congestion, and vehicle speed can influence pedestrians’ tendency to cross the road in front of AVs [6].

Computer vision plays a crucial role in enabling AVs to perceive their surrounding environment by analysing the visual



Fig. 1. Pedestrians’ crossing intention prediction in complex urban scenarios via contextual data analysis and a multi-camera perception setup.

data captured via multiple sensors, such as cameras, LiDAR, Radar, etc. Learning-based models, in particular deep neural networks (DNNs), have shown remarkable success in various computer vision tasks, including scene understanding, semantic segmentation [7], road users classification, localisation [8], and motion prediction [9]. Figure 1 illustrates some of the perceivable factors such as depth, pedestrian pose, and surrounding objects that an autonomous vehicle should consider to interpret the scene and estimate the pedestrians’ intention. DNNs are particularly effective at learning complex patterns and features from visual data, making them a natural fit for tasks that involve analysing images or videos to comprehend pedestrian behaviour [10]–[12]. They also offer significant capabilities in multi-modal integration by providing a neural-based mechanism to process and fuse all the perceived information from diverse sensors. This integration may enhance the overall understanding of the environment and help to make more accurate and safer decisions [13].

Several datasets, such as JAAD [14], PIE [15], and STIP [16], use onboard camera recordings and their data are publicly released for the study of pedestrians’ behaviour before and during road crossing. However, most of the current research works suffer from supplying a multi-camera in-cabin setup to leverage the benefits of sensor fusion and multi-modal perception. In addition to the above-mentioned datasets, some baseline approaches [17] have been also established for analysing the visual cues and signals that pedestrians emit through their body language and positioning. The approaches highlight the benefits of combining these features with contextual information. Contextual information may include factors such as the road’s location, the time of day, weather conditions, the presence of traffic signals or crosswalks, the type of road (urban, suburban,

rural), and the position and behaviour of other vehicles near the scene [18]. To the best of our knowledge, no extensive research has been conducted to understand and interpret such contextual details and their effects on pedestrian’s decision-making.

In this study, we propose a customised DNN-based framework, called “PIP-Net” that takes various features of pedestrians, the environment, and the ego-vehicle state into account, to learn the context of a crossing scenario and consequently predict the intention of pedestrians in real-world AV urban driving scenarios. The main contributions of this research are highlighted as follows:

- A novel feature fusion model is presented to integrate AV’s surrounding cameras and combine visual and non-visual modalities, as well as a hybrid feature map that incorporates depth and instance semantic information of each road user to comprehend the latent dynamics in the scene.
- Introducing the multi-camera “Urban-PIP dataset”, which includes various real-world scenarios of pedestrian crossing for autonomous driving in urban areas.
- We examine the effectiveness of the various input features, temporal prediction expansion, and the worthiness of expanding the vehicle field of view from one camera to three cameras based on the latest Waymo car camera setup [19] to ensure the developed model will be in line with the current technology developments in the AV industry.
- Finally, we evaluate the effectiveness of the proposed model on the widely utilised PIE dataset and the introduced Urban-PIP dataset, outperforming the state-of-the-art (SOTA) for predicting pedestrian actions [11].

II. RELATED WORKS

Recently, pedestrian crossing intention prediction research has surged and gained significant attention within the autonomous driving research community [10]–[12], [20]. Most current methods mainly address the problem by taking two aspects into account: Discovering influential factors and features for interpreting road users’ interactions [4]–[6], and designing the analytic model to predict the pedestrians’ crossing intention [14]–[18]. Both research directions mainly utilise advanced learning-based techniques. Deep learning methods have been fostered on multiple features of pedestrians and the environment, whether derived from annotations, visual information from videos or their combinations [2]. The following two subsections are dedicated to introducing approaches that utilise DNN-based architectures for spatio-temporal analysis and feature selection/fusion.

A. Spatio-temporal Analysis

Recently, there has been a shift from still image analysis to the incorporation of temporal information into the prediction models. Rather than relying on individual images, most contemporary methods utilise sequences of input images for decision-making by their prediction models. This adaptation recognises the significance of temporal data in enhancing the

prediction task, resulting in what is known as spatio-temporal modelling.

Spatio-temporal modelling can be achieved through a two-step process. Initially, visual (spatial) features per frame can be extracted using 2D convolutional neural networks (CNNs) [21] or graph convolution networks (GCNs) [16]. Subsequently, these extracted features are then fed into RNNs, such as the long short-term memory (LSTM) [15] or the gated recurrent unit (GRU) models [22]–[24]. For instance, in [25], [26], 2D convolutions are employed to extract visual features from image sequences, while RNNs encode the temporal relationships among these features. These sequentially encoded visual features are then inputted into a fully-connected layer to generate the ultimate intention prediction.

An alternative approach to extracting sequential visual features involves the utilisation of 3D CNNs (Conv3D) [27]. This technique directly captures spatio-temporal features by substituting the 2D kernels within the convolution and pooling layers of a 2D CNN with their 3D equivalents. For instance, in works such as [28] and [29], a framework based on a 3D CNN, specifically a 3D DenseNet, is employed to directly extract sequential visual features from sequences of pedestrian images. The ultimate prediction is then made using a fully-connected layer. Transformer architecture has also been utilised in another study [30] to tokenise the temporal input features and subsequently judge the pedestrians’ intention.

B. Feature Selection and Integration

Instead of pursuing an end-to-end approach for modelling visual features, it is possible to treat various types of information such as the pedestrian’s bounding box, body pose keypoints, vehicle movement, and the broader contextual backdrop as distinct input channels for the prediction model [12]. This necessitates the development of a fusion approach for amalgamating this diverse information.

The investigation into the types of features, such as pedestrians and environmental context, is still ongoing. For instance, pedestrian-to-vehicle distance is considered one of the most influential factors in pedestrians’ decision to cross [5]. This feature is typically estimated as a single measure between the target pedestrian and the ego vehicle [4]. Alternatively, a depth map of the scene (see Figure 2e) can be used to assess the distance from other road users and possibly reveal the underlying dynamics [31]. However, the depth map is susceptible to noise due to rough estimation, which can lead to inaccuracies in multiple pedestrian crossing scenarios [32].

Studies such as [33]–[35] have incorporated human poses or skeletons into pedestrian crossing prediction tasks, using pose keypoints extracted from pedestrian images to construct classifiers. This approach has shown improved prediction accuracy, but often neglects other important features or lacks attention to feature integration.

On the other hand, some studies specifically concentrated on feature integration. For instance, vision and non-vision branches fusion [36] suggest how to efficiently combine diverse data modalities at different stages of a DNN model to surge the intention prediction accuracy. Another study [10] is

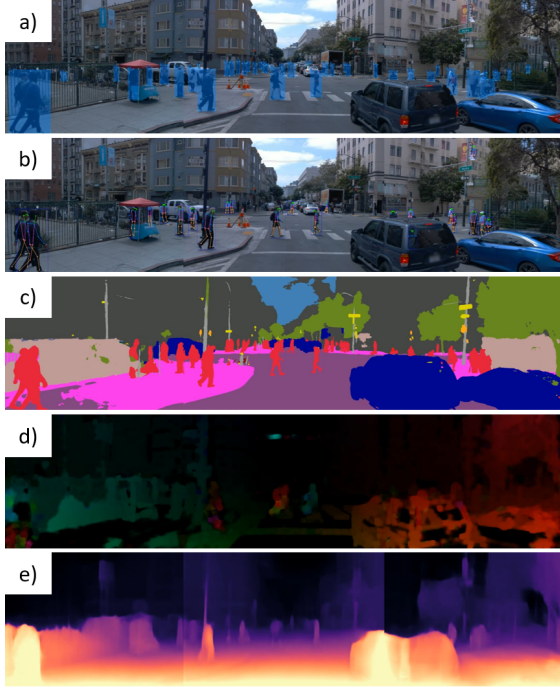


Fig. 2. Analysing pedestrians' features and traffic scene dynamics through: a) Pedestrian localisation, highlighted with bounding boxes, b) Gesture understanding with pose estimation, c) Object categorisation through segmentation, d) Understanding global motion patterns from optical flow, and e) Estimating distance via global depth heatmap.

conducted to merge two visual and three non-visual elements of the pedestrian, scene, and subject vehicle in a multi-stream network. From a different perspective, in studies such as [11], [37], local and global contextual information has been weighted by an attention mechanism [38] and fused together to apply a prediction on *Joint Attention in Autonomous Driving* (JAAD) [14] and *Pedestrian Intention Estimation* (PIE) [15] datasets.

C. Research Gaps

Pedestrian crossing intention highly relies on the distance of the AV to the pedestrian and the relative distance of the pedestrian to other road users which may fall into various categories of instance segmentation (e.g., cars, other pedestrians, etc.). None of the reviewed research has considered the simultaneous impact of both features on pedestrian intention.

On the other hand, to the best of our knowledge, no prior study has considered instance segmentation to smooth and normalise the distance measurement of road user instances.

In this article, we propose a new concept of *Categorical Depth* which integrates the classic noisy depth measurement with instance segmentation to gain more accurate depth information.

As another issue, the reviewed models, often have limited generalisability and are incapable of performing in the wild and real-world scenarios, as they have not been tested under authentic autonomous driving conditions [20]. Our study focuses on the real-world Waymo dataset which is collected from an AV's field of view.

Lastly, there is a shortage of dedicated neural network architectures capable of effectively accommodating and extracting maximal multi-camera information from around the AV for context recognition, hence an accurate model for predicting pedestrian crossing intentions. Camera integration is proposed in this study to cope with the limited field of view.

III. METHODOLOGY

We propose the PIP-Net prediction model, which is based on deep neural networks for predicting pedestrian crossing intention. The model incorporates spatial-temporal features such as road users' positioning, pose, and dynamic movements, along with a hybrid feature map that includes categorised semantic and depth information as input to the network. A multi-camera stitching and integration model is developed to facilitate panoramic viewing, enabling synchronised pedestrian ID assignment and tracking across the entire multi-view scene, thus enhancing the PIP-Net model's understanding of spatial characteristics and contextual information.

An overview of the proposed architecture is illustrated in Figure 3. The input features are categorised into spatial kinematic data and contextual data, and they are passed to the model through distinct pipelines based on their data types. Finally, we employ recurrent and attention modules to facilitate the processing of temporal data.

A. Spatial Kinematics

Kinematic input data includes the positioning of the pedestrian in the scene with reference to the detected pedestrian bounding box P_{bb} , pedestrian body pose keypoints P_{bp} , and the ego-vehicle speed V_s .

The data is arranged in a gated recurrent unit (GRU) layer [22], beginning with the *Bounding Box* feature P_{bb} . It indicates the location of the pedestrians which is detected through the customised You-Only-Look-Once algorithm for road user detection [39]. This feature is defined as:

$$P_{bb} = \{b_i^{t-m}, b_i^{t-m+1}, \dots, b_i^t\}, \quad (1)$$

where $b_i = [x_1, y_1, x_2, y_2] \in \mathbb{R}^4$ represents the coordinates of a pedestrian bounding box. It consists of the top-left ($[x_1, y_1]$) and the bottom-right coordinates ($[x_2, y_2]$). The dimension of the bounding box matrix P_{bb} is determined as $m \times 4$, where m is the observation time which indicates the number of frames that are observed to predict the pedestrian intention. We define t as the *decisive moment*, 0.5 ~ 4 seconds before the crossing event.

The *Body Pose* feature P_{bp} is defined as:

$$P_{bp} = \{p_i^{t-m}, p_i^{t-m+1}, \dots, p_i^t\}, \quad (2)$$

where the pose keypoints are obtained using YOLO-Pose [40], which estimates the pose of a person by detecting 17 keypoints joints, including the shoulders, elbows, wrists, hips, knees, ankles, eyes, ears, and nose. The keypoints are represented by a 34-dimensional vector, p_i , which contains the 2D coordinates of each joint for the i -th pedestrian at time t .

The *Vehicle Speed* is also defined as:

$$V_s = \{s_i^{t-m}, s_i^{t-m+1}, \dots, s_i^t\}, \quad (3)$$

where s_i refers to the exact speed of the ego-vehicle in *km*.

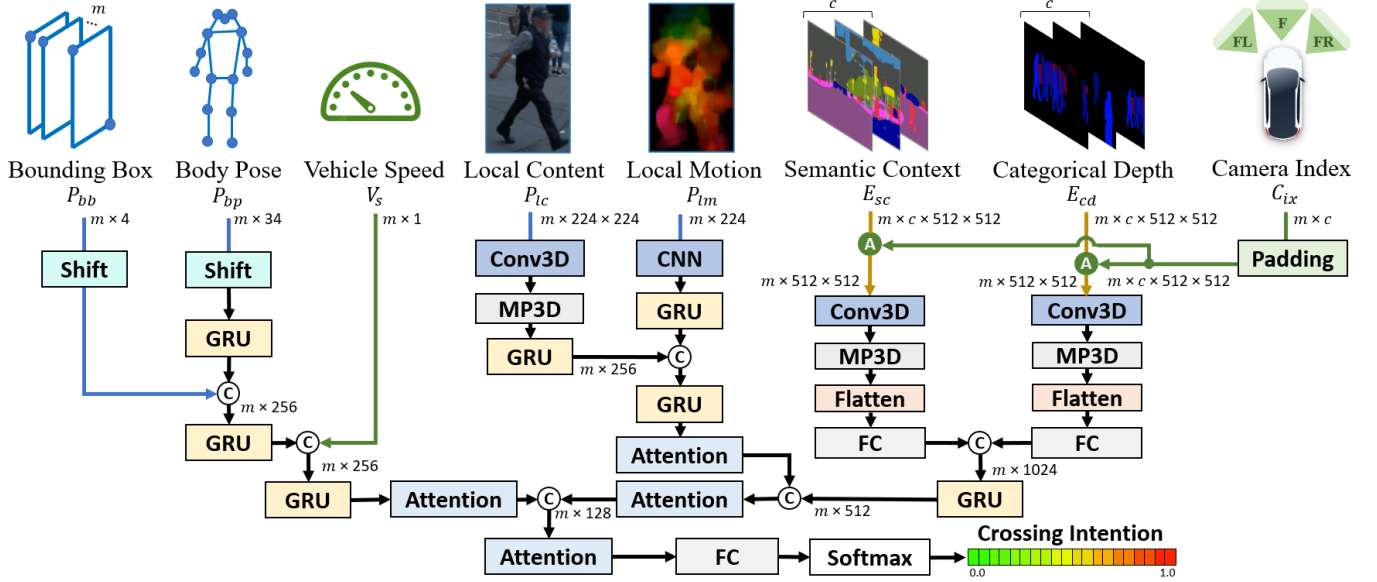


Fig. 3. The overview of the proposed DNN-based framework. PIP-Net receives *Spatial Kinematic* and *Spatial Context* data, and applies multi-modal feature fusion and multi-camera integration with temporal and attention-based analysis to predict pedestrians' crossing intentions. Shift and Padding units adjust the location of the target pedestrian with respect to the corresponding camera. Aggregation module (A) fuses the cameras' features as shown in Figure 5.

B. Spatial Context

Contextual input data includes pedestrian features, such as a pedestrian-bounded image (*Local Content*, P_{lc}) and corresponding motion flow analysis of the pedestrian (*Local Motion*, P_{lm}), the environment features like semantic segmentation of the scene (*Semantic Context*, E_{sc}), as well as our proposed hybrid feature map (*Categorical Depth*, E_{cd}), which refines depth information for specific pedestrians and vehicles in the scene. The mentioned features are obtained by using an ImageNet pre-trained VGG19 network as the backbone CNN, with a maximum pooling layer as suggested in [36]. Subsequently, a GRU is applied recursively to process each of these features.

The *Local Content* feature P_{lc} is defined as:

$$P_{lc} = \{lc_i^{t-m}, lc_i^{t-m+1}, \dots, lc_i^t\}, \quad (4)$$

where lc_i denotes the feature vector that is output by applying the CNN backbone to an RGB image. The image contains an individual pedestrian, cropped based on the bounding box location and subsequently warped to dimensions of $224 \times 224 \times 3$ pixels, which is the optimum spatial size in the network [30].

The resulting input feature vector is extracted as $(m, 512)$ via a Conv3D layer. It is then passed through a 3D max-pooling layer (MP3D) with a kernel size of 4×4 and a GRU module. This process yields a $(m, 128)$ vector, where m represents the observation time.

The *Local Motion* feature P_{lm} is derived from the dense optical flow analysis within the pedestrian-bounded image. This analysis is more consistent than examining the entire scene, which can be affected by ego-vehicle motions. We opt for a more advanced optical flow approach using FlowNet2 [41]. This deep learning-based method offers improved accuracy

and faster run-time performance. The *Local Motion* is defined as:

$$P_{lm} = \{lm_i^{t-m}, lm_i^{t-m+1}, \dots, lm_i^t\}, \quad (5)$$

where lm_i is considered as the localised i -th pedestrian motion descriptor. A CNN layer is used to extract a feature vector of size $(m, 256)$. This vector is then inputted into a GRU layer, resulting in an $(m, 128)$ vector, suitable for concatenation with the *Local Content* feature vector.

The *Semantic Context* feature E_{sc} is defined as:

$$E_{sc} = \{sc^{t-m}, sc^{t-m+1}, \dots, sc^t\}, \quad (6)$$

where sc refers to the semantic segmentation of objects within the entire scene encompassing road structure and users. This feature ensures that the model considers the spatial distribution of classes for both moving and static objects within the scene. The semantic information is extracted by Slot-VPS [42] model, which is a panoptic video segmentation algorithm that not only offers semantic segments but also a unique ID for each instance of the objects in the scene. The segmented classes include 8 dynamic classes (person, rider, car, truck, bus, train, motorcycle, and bicycle) and 11 static classes (traffic light, fire hydrant, stop sign, parking meter, bench, handbag, road, sidewalk, sky, building, and vegetation).

The *Categorical Depth* feature E_{cd} is defined as:

$$E_{cd} = \{cd^{t-m}, cd^{t-m+1}, \dots, cd^t\}, \quad (7)$$

where cd represents the hybrid feature map showing the spatial distribution and distance of various instances of pedestrians and vehicles within the scene. The depth data are initially estimated using the ManyDepth model [43] and encoded in a heatmap representation, resulting in a global depth heatmap. As illustrated in Figure 2e, high-intensity spots (white and

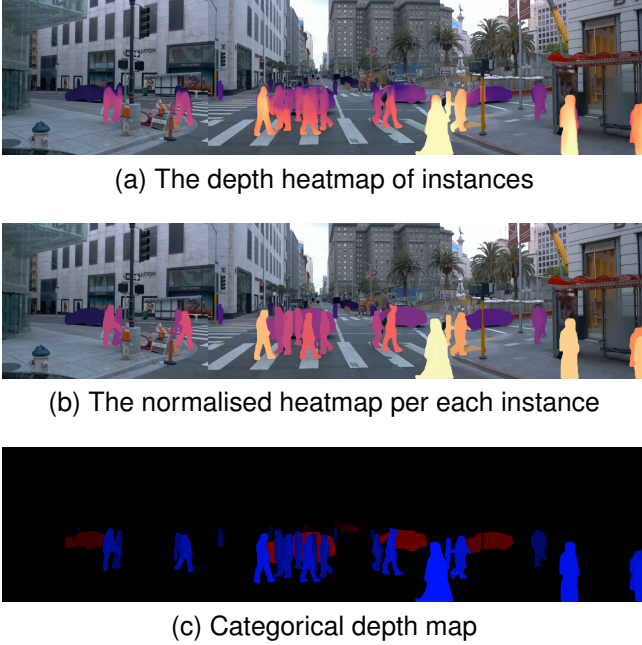


Fig. 4. **Colour-coded visualisation of road users' distance to the ego-vehicle after the tripe camera stitching.** 4a is the proportion of the global depth heatmap which pedestrians and vehicles occupy; 4b is the normalised heatmap values per each instance; 4c is a visualised E_{cd} feature in an RGB format in which pedestrians and vehicles integrated into the blue and red channel, respectively, and high-intensity values indicate closer users. A categorical depth map has a positive effect on removing the camera stitching effect and increasing the clarity and saliency of pedestrians and vehicles in the scene.

oranges) indicate proximity to the ego vehicle, while low-intensity spots (navy blue and black) represent greater distances. However, our experiments revealed that the global depth heatmap is unreliable due to inconsistencies in providing clear object boundaries. To address this, the pedestrian and vehicle instances are cropped using instance masks obtained from the Slot-VPS, as shown in Figure 4a. Subsequently, the intensity of pixels within each instance is normalised by averaging, yielding a normalised heatmap as seen in Figure 4b. This process ensures a clear and consistent depth estimation for each instance of classes, as depicted in Figure 4c.

Both inputs, E_{sc} and E_{cd} , undergo extraction via a Conv3D layer to be assessed for the spatio-temporal analysis. The feature dimensions are gradually reduced ($512 \rightarrow 256 \rightarrow \dots \rightarrow 64$) by repeatedly subjecting them to max-pooling layers. This process not only selects the most important information from the local neighbourhood of each pooling window but also reduces the spatial dimensions (width and height) of the feature maps and the computational complexity of the network. Then the features are organised using a flattened layer, resulting in a one-dimensional array that is suitable for concatenation and can be fed into a fully-connected layer (FC). Finally, the data is passed through a GRU module. The outputs of the three GRUs are combined and concatenated into a single output, which is then passed through an attention mechanism.

C. Cameras Features Integration

The incorporation of multiple cameras might be beneficial for capturing complex traffic scenarios, such as intersections,

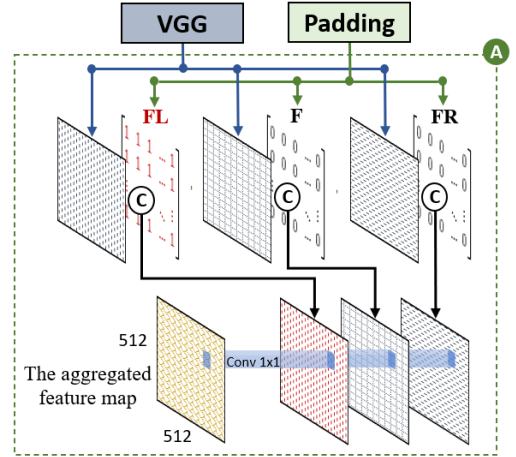


Fig. 5. **The multi-camera feature aggregation module.** In this example, the front-left camera (FL) is the sentinel camera, where the target pedestrian is observed. The padding module expands the *Camera Index* value and provides a camera indicator mask for combining with *Sense Context* and *Categorical Depth* features.

thanks to providing a surrounding field of view. In these scenarios, pedestrians may approach the road from the sides rather than directly in front of the vehicle. They may also choose to cross the road while a vehicle is changing lanes or making a turn. By incorporating left and right-side cameras, we can gather critical information about pedestrians in adjacent lanes or at the side of the vehicle. The Waymo dataset is one of the best options with three cameras ($c = 3$) that also offer a diversity of real-world pedestrian crossing scenarios. The cameras are named front-left (FL), front (F), and front-right (FR) positioned from the AV's left to right angles (as shown in Figure 2). The synchronised videos provided have an approximately 11% overlap along the edges. These overlapping areas can introduce redundancy in data and make it challenging to precisely determine the pedestrian's position, movement, and intention when it moves from one camera scene to another. Therefore, we merge the cameras using the Panoptic stitching over time approach [19], excluding the overlapping regions and giving higher priority to the front-view camera. Figure 2 illustrates an example of different types of features that have been extracted from three cameras, and then stitched together to constitute a single wide image.

We define *Sentinel Camera* as a variable that indicates the index of the camera (C_{ix}) on which the target pedestrian has been observed. Using the *Camera Index*, we can adjust the pose and bounding box coordinates with respect to the sentinel camera. This task will be accomplished by the Shift unit, as shown in Figure 3 in cyan, which extends the global coordinates from the leftmost camera to the rightmost one, and applies these adjustments to the inputs. In this context, the Padding unit is responsible for generating a zero binary mask of size $c \times 512 \times 512$, where the c -th dimension corresponds to the sentinel camera being set to one. Here, c represents the number of cameras. As the aggregation module (A) shown in Figure 5, the binary masks are combined with the feature vectors generated by the VGG19 network for each E_{sc} and E_{cd} . Subsequently, a pointwise convolution (Conv

1×1) operator aggregates all the features across cameras. This process combines features from different channels (cameras) at each spatial location, allowing a weighted combination of input features.

D. Temporal and Attention Module

To account for the temporal context of input features, GRU is employed. When describing the recursion for the GRU equation, the variables at the j -th level of the stack can be outlined as follows:

$$z_j^t = \sigma(x_j^t W_j^{xz} + h_j^t W_j^{hz} + b_j^z), \quad (8)$$

$$r_j^t = \sigma(x_j^t W_j^{xr} + h_j^t W_j^{hr} + b_j^r), \quad (9)$$

$$\tilde{h}_j^t = \tanh(x_j^t W_j^x + (r_j^t \odot r_j^{t-1}) W_j^h + b), \quad (10)$$

$$h_j^t = (1 - z_j^t) \odot h_j^{t-1} + z_j^t \odot \tilde{h}_j^t, \quad (11)$$

where $\sigma(\cdot)$ denotes the logistic sigmoid function x_j^t is the input feature at time step t . The reset and update gates at time step t are denoted as r_j^t and z_j^t , respectively, and the weights between the two units are represented by W . The hidden state at the previous time step and the current time step are represented by h_j^{t-1} and h_j^t , respectively.

To assess the significance of the processed features during network training, the attention mechanism [38]) is utilised to focus on specific segments of features, thereby enhancing the effectiveness of feature analysis. The resulting vector from the attention module is defined as follows:

$$A = \tanh(W_c[h_c : h_m]), \quad (12)$$

$$h_c = \sum_{s^t} \alpha^t h_{s^t}, \quad (13)$$

where W_c represents a weight matrix, h_c denotes the cumulative sum of all attention-weighted hidden states, h_m signifies the final hidden state of the encoder, h_{s^t} corresponds to the preceding hidden state of the encoder, and α^t denotes the vector of attention weights, which is defined as follows:

$$\alpha_t = \frac{\exp(\text{score}(h_m, \tilde{h}_s))}{\sum_{s^t=1}^{t_m} \exp(\text{score}(h_m, \tilde{h}_{s^t}))}, \quad (14)$$

$$\text{score}(h_m, h_{s^t}) = h_m^T W_p h_{s^t} \quad (15)$$

where t_m is the input sequence length at time t . h_m^T represents the transpose of the h_m vector, and W_p is a weight matrix that can be estimated through the training phase of the network.

In the tile of the network, the outputs of the attention modules are concatenated and then forwarded through the last attention module and an FC layer. The ultimate output, normalised to a range between zero and one using the Softmax function, represents the prediction for pedestrian crossing intention.

IV. EXPERIMENTS

In this section, we conduct four distinct experiments to thoroughly assess the robustness of the proposed framework. Each experiment is designed to provide unique insights into various aspects of the model's performance. We compare our model against the PIE dataset in four different intervals

TABLE I
DATASET SPECIFICATIONS

| Specification | PIE | Urban-PIP |
|----------------------------------|---------|-------------------|
| Autonomous Driving | No | Yes |
| Number of Cameras | 1 | 3 |
| Auxiliary Sensors | OBD | LiDAR, Radar, IMU |
| Video clip lengths | 10 min | 16 sec |
| Total Number of Frames | 909,000 | 32,790 |
| Total Number of Annotated Frames | 293,000 | 32,790 |
| Total Number of Pedestrians | 1,842 | 1,481 |
| Crossed Pedestrians | 512 | 409 |
| Not Crossed Pedestrians | 1,328 | 1,072 |

ranging from 1 to 4 seconds, allowing us to scrutinise the model's predictive capabilities for an in-time response in different driving scenarios. The second experiment examines the impact of the introduced Categorical Depth and Local Motion features in enhancing the framework's prediction accuracy. The third experiment evaluates the model's generalisability and reliability on a diverse dataset from Waymo's self-driving vehicles. This investigation ensures that the framework performs effectively across different real-world scenarios. Lastly, we investigate the scalability of the model by assessing the framework's ability to handle one to three cameras simultaneously, expanding its view angles. This provides insights into the model's efficiency when processing information from multiple cameras. This multi-faceted evaluation allows us to gain a detailed understanding of the model's effectiveness, in comparison to a singular experiment.

A. Datasets

The JAAD [14] and STIP [16] datasets suffer from no annotation in terms of ego-vehicle speed values. Furthermore, there is a slight bias in these datasets, as the majority of annotations indicate the cases of crossing which may not result in effective training of deep models. Therefore, the evaluations were conducted on the *Pedestrian Intention Estimation* (PIE) [15] dataset, which is extensively employed in the majority of prior studies. Additionally, we utilised our custom dataset named Urban-PIP, specifically annotated for pedestrian crossing behaviour, built upon the Waymo [19] dataset. Waymo is a widely used dataset for traffic perception by AVs thanks to the diversity of the video data from urban and rural environments under various driving conditions and situations. The specifications of datasets are briefly mentioned in Table I.

1) **PIE dataset:** The dataset is recorded on a sunny clear day for 6 hours in HD format (1920×1080). Each video segment lasts approximately 10 minutes, resulting in a total of 6 sets. We utilised approximately 50% (880 samples) of the dataset for training, 40% (719) for testing, and 10% (243) for validation as per the same split proportion as [11]. Regarding occlusion levels, partial occlusion is defined when an object is obstructed between 25% and 75%, while full occlusion occurs when the object is obstructed by 75% or more. The dataset includes the vehicle speed, heading direction, and GPS coordinates.

2) **Urban-PIP dataset:** The dataset is recorded under various weather and daytime conditions in three geographical

locations using a multi-sensor setup. This multi-modal dataset is collected via a combination of LiDAR, cameras, radar, and IMU sensors mounted on the ego-vehicle. LiDAR provides 360° field of view with approximately a 300-meter range by beaming out millions of laser pulses per second and measuring the time of laser beam flight from the sensor to the surface of an object, then reflecting from the object to the sensor on the ego-vehicle. The radar system has a continuous 360° view to track the presence and speed of road users in front, behind and sides of the vehicle. The front cameras (FL, F, and FR) simultaneously capture the traffic scene videos in HD format (1920 × 1080). The IMU module uses accelerometers and gyroscopes with input from GPS, maps, wheel speeds, as well as laser and radar measurements to provide position, velocity, and heading information to the vehicle.

In this study, the experiments are conducted using camera sensors as they provide rich visual information, including detailed information about pedestrian behaviour, body language, and contextual information that can be crucial for predicting crossing intentions. Also, the affordability of camera sensors has made them a practical choice for current research on intention prediction. We annotated 1,481 pedestrian crossing intentions from the front cameras including 448 in the front-left camera, 541 from the front camera, and 492 from the front-right camera.

To assess models limited to a single camera, we introduce a subset, named *Frontal-Urban-PIP*, focusing on pedestrians observed only by the front camera. This subset, featuring 55 pedestrians with crossing intentions and 129 without, ensures a fair comparison will be conducted with similar methods which are limited to a single camera only.

B. Implementation Settings

The proposed model was executed on a CUDA parallel computing platform with an Nvidia Quadro RTX A6000 GPU and Intel Core i9 13900K 24-core processor and the Torch environment. PIP-Net was trained using the RMSProp optimiser. 256 hidden units were used for the GRUs, and the sigmoid (σ) activation function was applied to the GRUs for handling spatial kinematic data. To mitigate overfitting, a dropout rate of 0.5 was introduced after the attention block. Additionally, an L2 regularisation term of 0.0001 was incorporated into the last fully connected layer. A stride of 3 steps is used for each input sequence in the observation scene, resulting in a total of 10 frames for one second. This stride reduces frame redundancy and compensates for feature extraction time delay.

PIP-Net- α : This model is designed for a single camera setup. The model is trained on the PIE dataset and also evaluated against the PIE test set and Frontal-Urban-PIP datasets. The model doesn't have the Camera Index pipeline within its architecture. Thereby, the outputs of the Max-pooling 3D (MP3D in Figure 3) are directly forwarded to the flattened block, and the Shift blocks are deactivated. A learning rate of 5×10^{-5} was used for 300 epochs with a batch size 10. The model was tested on the Frontal-Urban-PIP dataset to evaluate its generalisability. The input length stride was set to 1 because the dataset's FPS was already equal to 10.

TABLE II
SOTA PERFORMANCE COMPARISON ON THE PIE DATASET.

| Model | Acc | AUC | F1 | Precision | Recall |
|---|-------------|-------------|-------------|-------------|-------------|
| ATGC (2017) | 0.59 | 0.55 | 0.39 | 0.33 | 0.47 |
| Multi-RNN (2018) | 0.83 | 0.80 | 0.71 | 0.69 | 0.73 |
| SingleRNN (2020) | 0.81 | 0.75 | 0.64 | 0.67 | 0.61 |
| SFRNN (2020) | 0.82 | 0.79 | 0.69 | 0.67 | 0.70 |
| PCPA (2021) | 0.87 | 0.86 | 0.77 | 0.75 | 0.79 |
| CAPformer (2021) | 0.88 | 0.80 | 0.71 | 0.69 | 0.74 |
| PPCI (2022) | 0.89 | 0.86 | 0.80 | 0.79 | 0.81 |
| GraphPlus (2022) | 0.89 | 0.90 | 0.81 | 0.83 | 0.79 |
| MCIP (2022) | 0.89 | 0.87 | 0.81 | 0.81 | 0.81 |
| CIPF (2023) | 0.91 | 0.89 | 0.84 | 0.85 | 0.83 |
| PIP-Net-α (Ours) | 0.91 | 0.90 | 0.84 | 0.85 | 0.84 |

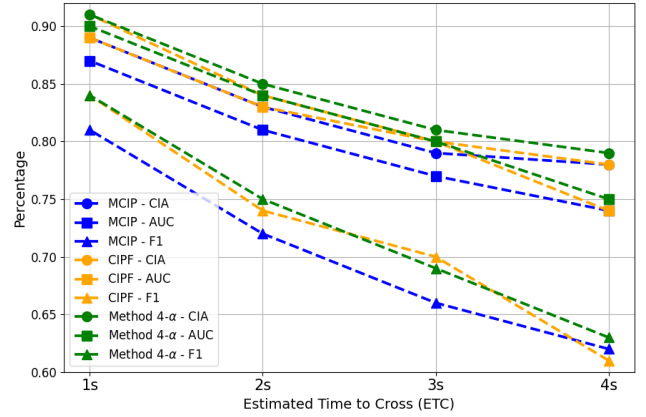


Fig. 6. Comparative analysis of prediction performance is conducted for future time points in the study. Models are evaluated in terms of their predictive accuracy from 1 second to 4 seconds ahead.

PIP-Net- β : This model is designed for multi-camera setups to be evaluated against Urban-PIP with three cameras. The training of this model is performed using the Urban-PIP dataset with various observation times, a learning rate of 4×10^{-5} across 400 epochs, and a batch size of 6. The split ratio for training and testing samples is 80% (1,181 samples) and 20% (296 samples) of the dataset, respectively.

C. Comparative Results

Table II highlights the performance of our method on the PIE dataset. The observation time (m) has been set to 16 frames, the same as the previous methods to ensure a fair comparison with other methods. PIP-Net- α , achieves the highest values in all metrics, showcasing its prowess in capturing the crossing intention classification. These metrics include *accuracy* (Acc), *precision*, and *recall rate*, which quantify the model's ability to accurately predict the binary classification task. Additionally, the *area under the ROC curve* (AUC), indicates the model's proficiency in distinguishing between different classes, and *F1 score*, represents the harmonic mean of precision and recall rate.

In comparison to MultiRNN [24], SingleRNN [25], and SFRNN [23] models, which use a CNN encoder for visual features and RNN-based encoder-decoder structure, PIP-Net- α shows significant improvements by considering a new combination of input features. Transformer and graph-based architectures used in CAPformer [30] and GraphPlus [35] models

TABLE III

PIP-Net- α SUB-VARIANTS USING DIFFERENT INPUT FEATURES ON THE PIE DATASET. ABBREVIATIONS ARE: LM: LOCAL MOTION, GM: GLOBAL MOTION, GD: GLOBAL DEPTH, AND CD: CATEGORICAL DEPTH. THE UP ARROW INDICATES AN IMPROVEMENT AND THE DOWN ARROW INDICATES A DECREMENT IN COMPARISON WITH THE BASELINE VARIANT.

| Model | GM | LM | GD | CD | Acc | AUC | F1 |
|------------|----|----|----|----|---------------|---------------|---------------|
| α^0 | - | - | - | - | 0.883 | 0.875 | 0.792 |
| α^1 | ✓ | - | - | - | 0.892↑ | 0.881↑ | 0.789↓ |
| α^2 | - | ✓ | - | - | 0.889↑ | 0.887↑ | 0.801↑ |
| α^3 | - | - | ✓ | - | 0.877↓ | 0.870↓ | 0.798↑ |
| α^4 | - | - | - | ✓ | 0.904↑ | 0.892↑ | 0.829↑ |
| α^5 | ✓ | - | ✓ | - | 0.875↓ | 0.871↓ | 0.789↓ |
| α | - | ✓ | - | ✓ | 0.911 | 0.903 | 0.844 |

have been less effective compared to PIP-Net with RNN-based architecture. The proposed feature fusion approach using seven input features, including three kinematic features and four contextual features, has also improved AUC by +1% compared to CIPF [11], which integrates eight distinct input features derived from pedestrians and vehicles through three fusion modules.

1) *Crossing time prediction*: Depending on the traffic scenario, the model’s prediction performance may vary. The model can predict the pedestrians’ estimated time to cross (ETC), 1 to 4 seconds in advance. For example, an ETC = 2 means the model expects or predicts the target pedestrian crosses in 2 seconds.

We evaluated the performance of the proposed PIP-Net- α model across various ETCs from 1 to 4 seconds. Figure 6 presents a comparison of the Acc, AUC, and F1 performance of PIP-Net- α with two recent prediction models, CIPF and MCIP, using the PIE dataset. All three models exhibited a decline in performance across all metrics as the Estimated Time to Cross (ETC) increased, i.e. when the models tried to have a longer-term prediction. Notably, the most significant drop in AUC occurred between the ETC = 1-second and ETC = 2, with MCIP and CIPF models decreasing by 6.8% and 6.7%, respectively. This is while our model shows a 6.6% decrease in the AUC from ETC = 1 to 2. The Accuracy also shows gradual decreases from the 3-second to the 4-second interval, with all models experiencing a decrease of approximately 1% (MCIP) and 2% (CIPF), respectively. As can be seen, the proposed model with green dashed lines consistently outperformed the other models for all ETCs.

2) *Features Importance*: Recent studies [10]–[12], [30] have emphasised the importance and reliability of primary features including *Bounding Box*, *Body Pose*, *Local Content*, *Vehicle Speed* and *Semantic Context*, in their elaborate experiments. The baseline model, α^0 , comprises these primary features.

Initial experiments have demonstrated that excluding the input of the *Bounding Box* leads to 8.6% decrease in accuracy compared with the baseline. While omitting the *Body Pose* parameter only reduces accuracy by 3.5%. This represents less importance of body pose compared to the bounding box which may seem counter-intuitive. However, our further investigations confirm the bounding box data is notably more important and useful as it includes the pedestrian’s moving trajectory and

TABLE IV

THE COMPARISON TABLE FOR THE FRONTAL-URBAN-PIP DATASET.

| Model | Acc | AUC | F1 | Precision | Recall |
|---|-------------|-------------|-------------|-------------|-------------|
| ATGC | 0.52 | 0.51 | 0.35 | 0.32 | 0.44 |
| Multi-RNN | 0.64 | 0.63 | 0.49 | 0.51 | 0.48 |
| SingleRNN | 0.65 | 0.64 | 0.54 | 0.57 | 0.53 |
| SFRNN | 0.65 | 0.65 | 0.55 | 0.58 | 0.53 |
| PCPA | 0.62 | 0.60 | 0.58 | 0.51 | 0.47 |
| PPCI | 0.63 | 0.61 | 0.59 | 0.52 | 0.47 |
| CAPformer | 0.64 | 0.60 | 0.55 | 0.58 | 0.54 |
| GraphPlus | 0.64 | 0.61 | 0.57 | 0.59 | 0.56 |
| PIP-Net-α (Ours) | 0.73 | 0.71 | 0.69 | 0.70 | 0.68 |

tracking history over time, providing valuable spatio-temporal information. While body poses spatio-temporal information is not very important. The body pose only seems to matter when the pedestrian is about to cross the road in the last few frames before crossing. Otherwise, the body pose in previous moments, such as when the pedestrian is on the sidewalk, is redundant.

Interestingly, removing the *Vehicle Speed* feature results in a 3.8% drop in accuracy, making it the second most important input. This aligns with the findings of the study by [30], which states that a model trained with the ego-vehicle speed tends to focus on the ego-vehicle speed adjustment (e.g. deceleration) to learn the pedestrian intention, rather than learning to predict the intention from the pedestrian behaviour.

Excluding *Semantic Context* leads to a 3.4% accuracy decrease as it includes details about road layout such as sidewalk positioning and drivable zones. The impact of removing *Local Content* is minor, causing accuracy to decrease by 1.7%. It appears to lack comprehensive features on pedestrians’ intentions, given the wide variety in appearance and accessories they may have.

Table III shows a comparison of the two input features we have used in the proposed model, which correspond to the scene motion and depth information. The α^2 demonstrates that the local motion feature can exhibit superior performance when compared to the global motion feature (2d), which includes optical flow analysis of the entire scene. While optical flow is typically sensitive to any movement between consecutive frames, it appears that local motion can provide a coarse-grained feature and treat more concisely to account pedestrians’ velocity and direction of movement, regardless of other irrelevant objects in the surroundings.

Regarding depth information features, the categorical depth feature proposed stands out as the most effective standalone feature, as evidenced by the results of α^4 in Table III, highlighting the importance of pedestrian group densities, their distances from the ego-vehicle, and interactions with other road users in the traffic scene. Conversely, α^3 performs the weakest among the sub-variants when compared with the baseline, which utilises the global depth heatmap of the entire scene (2e). This underperformance may be attributed to the unstable estimation of depth for irrelevant surrounding objects. This is addressed in the categorical depth by focusing only on pedestrians and vehicles, and then applying per-instance normalisation (as shown in Figure 4).

Finally, the optimal outcome is attained by taking into

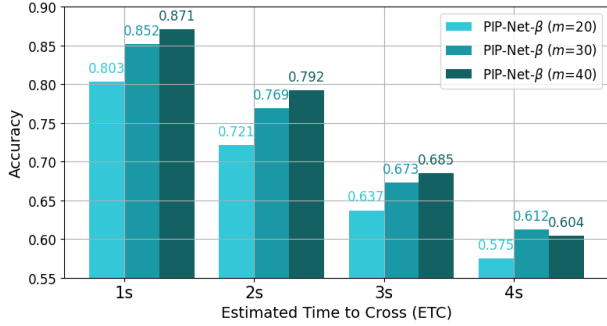


Fig. 7. Comparison of the crossing intention accuracy (Acc) for PIP-Net- β models (in three cameras mode) across various future time intervals, highlighting the disparities in performance at each observation time (m). The results are based on the Urban-PIP dataset.

account both the local motion and categorical depth map, leading to enhancements in the baseline regarding Acc, AUC, and F1 score by 1.8%, 3.1%, and 6.1%, respectively.

3) **Generalisation:** The PIP-Net- α evaluation is presented against the SOTA methodologies on the Frontal-Urban-PIP dataset in Table IV. Notably, the models have never seen the scenarios in their training phase. The outcomes of other methods were generated using the pre-trained weights they provided. Overall, the majority of models demonstrate improvements over ATGC across various metrics, with each model exhibiting its unique strengths. However, we witnessed a decrement in terms of performance for PCPA, PPCI, CAP-former, and GraphPlus. As far as the research curiosity demand, we investigated the architecture of these models, and it turned out they are suffering from low-quality global context and body pose features. This is caused by the feature extractor algorithms, i.e., semantic segmentation and pose estimator, they have used which hinder the classifier from judging based on precise features.

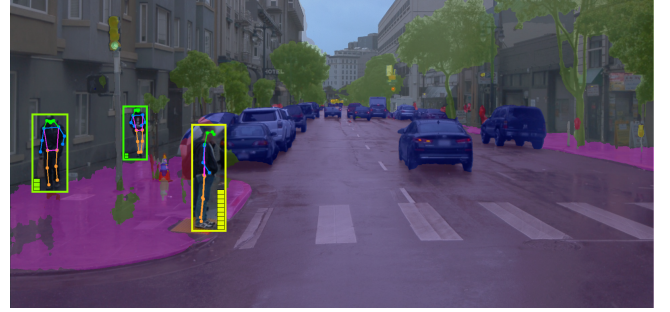
4) **View Angle Expansion:** We explored the enhancement of the field of view using three cameras to enable the autonomous vehicle to perceive a larger portion of its surroundings. For this purpose, we train PIP-Net- β with three different observation times (m) of 20, 30, and 40 frames. Subsequently, we examined how the prediction performance evolves as we expand the ETC prediction horizon from 1 to 4 seconds. As depicted in Figure 7, the accuracy of crossing intention prediction decreases as the ETC prediction expands. However, the accuracy often increases with the enlargement of observation time. Intriguingly, when ETC = 4 and $m = 40$ the accuracy was lower compared to $m = 30$. This discrepancy arises from the model predicting pedestrians to be crossing based on long-term observations when, in reality, they did not cross. This highlights the observation that a pedestrian’s previous actions do not always accurately indicate their future intentions, as they can change their mind and act in an instant [3].

D. Observational Results

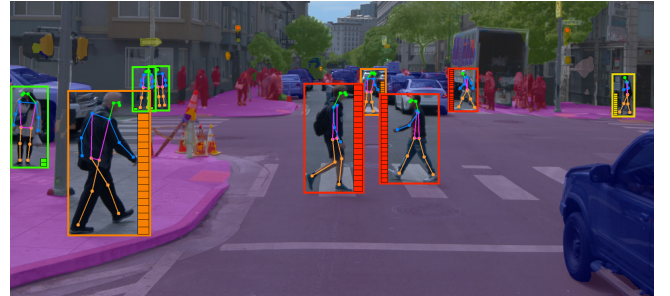
We present the qualitative results of the PIP-Net- α network in Figure 8 for Frontal-Urban-PIP datasets and in Figure 9 for



(a) A non-signalised junction



(b) A signalised junction with a green light



(c) A signalised junction with a red light

Fig. 8. A representation of the proposed model’s analysis on traffic video scenes of Frontal-Urban-PIP dataset. Three distinct images showcase intersections and traffic light conditions with confidence bars positioned in front of pedestrians, aligning with their body pose direction. These confidence bars visually indicate the model’s confidence about the crossing intention of the detected pedestrians for the upcoming 2-4 seconds into the future.

the PIE dataset. The intention is represented by a confidence bar, where higher values (reddish colour) indicate a high probability of the pedestrian crossing. Pedestrians without the intention to cross are depicted with greenish bounding boxes and lower values on the confidence bar.

We displayed frames from the past $t - 90$ frames to the t frame, where t represents the decisive moment. As the frames change, the prediction results for the pedestrian’s crossing intention also evolve. Some pedestrians are predicted to continue crossing, while others are forecasted to transition from not crossing to crossing, or vice versa, depending on the pedestrian’s direction or situation. For instance, the proposed model can predict the intention of the pedestrian in case 7, as shown in Figure 9, when the ego vehicle is going to turn left and the pedestrian tends to cross. The contextual information alongside pedestrian features like motions and direction of movements, seems to be crucial for accurately predicting their

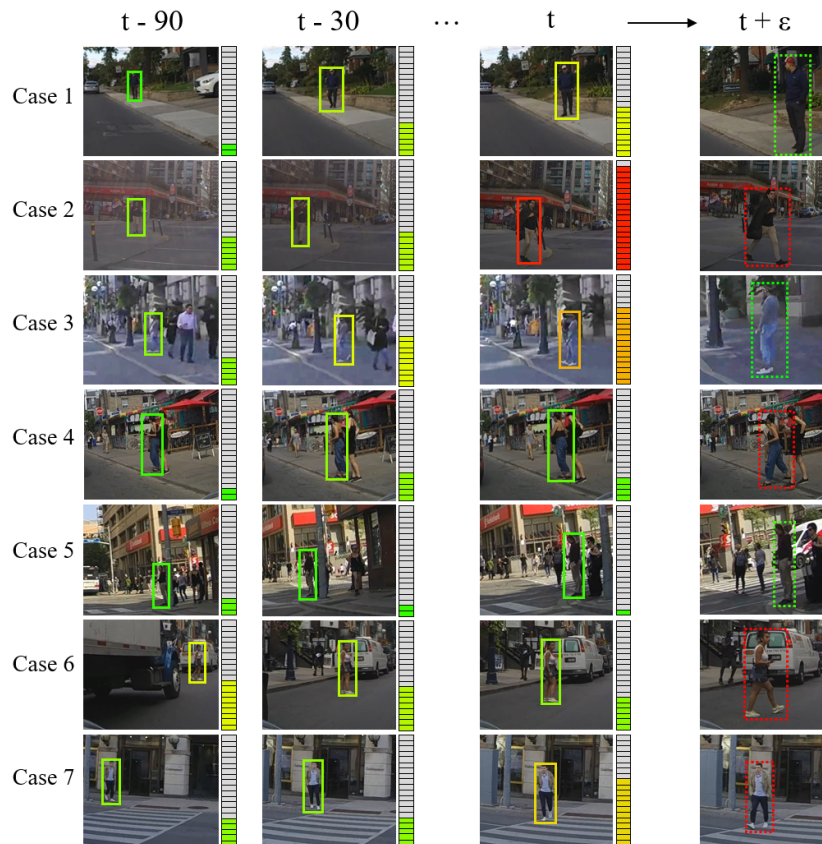


Fig. 9. Qualitative results of PIP-Net- α , ($m = 30$) on the PIE dataset. The pedestrian with a crossing intention has shown a higher value in the confidence bar. We demonstrate the past frame $t - 90 \sim t$ and the ground truth as a time in the future ($t + \epsilon$) with dashed bounding boxes, where red: cross, green: not cross.

behaviour in a given context.

V. CONCLUSION

This paper presented a framework called PIP-Net for predicting pedestrian crossing intentions in real-world urban self-driving situations. Two variants, α and β , were introduced to support different camera setups. By utilising both kinematic data and spatial features of the driving scene, the proposed model employed recurrent and temporal attention-based methodology to predict pedestrians' future crossing intentions accurately. Through quantitative and qualitative experiments on the PIE dataset, the proposed model achieved state-of-the-art performance with a 91% accuracy and an 84% recall rate.

The Urban-PIP was introduced as a new dataset for the pedestrian intention prediction task, including various AV driving scenarios and comprehensive annotations on a multi-sensory setup, thereby enabling a better future investigation of crossing behaviour studies. Our model demonstrated a generalisation capability when applied to the Urban-PIP dataset by +9%, +10%, and 12% improvement compared with other models in terms of accuracy, AUC, and F1 score, respectively. This was underlined by the scene feature extractors employed in training our model.

To enhance the visual encoding of road users and their relative distances to the ego vehicle, we introduced a categorical depth feature map. This, combined with the local motion flow

feature, provided salient information about the dynamics of the scene. Our results reveal that they cumulatively enhanced the accuracy and F1 score of the baseline model by +2.8% and +5.2%, respectively. Additionally, we investigated the impact of expanding the view angle using three cameras and enlarging prior observation frames.

Our algorithm achieved 85.4% accuracy in predicting pedestrian crossing intentions 2 seconds in advance and 79.3% accuracy for predictions between 2 and 4 seconds in advance. However, the algorithm is sensitive to the quality and precision of the input features, specifically, scene context and body pose information.

We anticipate that this algorithm can effectively prevent traffic accidents and protect vulnerable road users by foreseeing the crossing behaviour of nearby pedestrians.

REFERENCES

- [1] G. Yannis, D. Nikolaou, A. Laiou, Y. A. Stürmer, I. Buttler, and D. Jankowska-Karpa, "Vulnerable road users: Cross-cultural perspectives on performance and attitudes," *IATSS research*, vol. 44, no. 3, pp. 220–229, 2020.
- [2] N. Sharma, C. Dhiman, and S. Indu, "Pedestrian intention prediction for autonomous vehicles: A comprehensive survey," *Neurocomputing*, 2022.
- [3] A. Najmi, T. Waller, M. Memarpour, D. Nair, and T. H. Rashidi, "A human behaviour model and its implications in the transport context," *Transportation research interdisciplinary perspectives*, vol. 18, p. 100800, 2023.

- [4] Z. Zhou, Y. Liu, B. Liu, M. Ouyang, and R. Tang, "Pedestrian crossing intention prediction model considering social interaction between multi-pedestrians and multi-vehicles," *Transportation Research Record*, p. 03611981231187643, 2023.
- [5] A. H. Kalantari, Y. Yang, J. G. de Pedro, Y. M. Lee, A. Horrobin, A. Solernou, C. Holmes, N. Merat, and G. Markkula, "Who goes first? a distributed simulator study of vehicle-pedestrian interaction," *Accident Analysis & Prevention*, vol. 186, p. 107050, 2023.
- [6] B. Yang, W. Zhan, P. Wang, C. Chan, Y. Cai, and N. Wang, "Crossing or not? context-based recognition of pedestrian crossing intention in the urban environment," *IEEE Transactions on Intelligent Transportation Systems*, vol. 23, no. 6, pp. 5338–5349, 2021.
- [7] K. Muhammad, T. Hussain, H. Ullah, J. Del Ser, M. Rezaei, N. Kumar, M. Hijji, P. Bellavista, and V. H. C. de Albuquerque, "Vision-based semantic segmentation in scene understanding for autonomous driving: Recent achievements, challenges, and outlooks," *IEEE Transactions on Intelligent Transportation Systems*, 2022.
- [8] L. Chen, S. Lin, X. Lu, D. Cao, H. Wu, C. Guo, C. Liu, and F.-Y. Wang, "Deep neural network based vehicle and pedestrian detection for autonomous driving: A survey," *IEEE Transactions on Intelligent Transportation Systems*, vol. 22, no. 6, pp. 3234–3246, 2021.
- [9] M. Gulzar, Y. Muhammad, and N. Muhammad, "A survey on motion prediction of pedestrians and vehicles for autonomous driving," *IEEE Access*, vol. 9, pp. 137 957–137 969, 2021.
- [10] J.-S. Ham, K. Bae, and J. Moon, "MCIP: Multi-stream network for pedestrian crossing intention prediction," in *Computer Vision—ECCV 2022 Workshops: Tel Aviv, Israel, October 23–27, 2022, Proceedings, Part I*. Springer, 2022, pp. 663–679.
- [11] J.-S. Ham, D. H. Kim, N. Jung, and J. Moon, "CIPF: Crossing intention prediction network based on feature fusion modules for improving pedestrian safety," in *Proceedings of the IEEE/CVF Conference on Computer Vision and Pattern Recognition*, 2023, pp. 3665–3674.
- [12] R. Ni, B. Yang, Z. Wei, H. Hu, and C. Yang, "Pedestrians crossing intention anticipation based on dual-channel action recognition and hierarchical environmental context," *IET Intelligent Transport Systems*, vol. 17, no. 2, pp. 255–269, 2023.
- [13] T. Zhang, X. Chen, Y. Wang, Y. Wang, and H. Zhao, "Mutr3d: A multi-camera tracking framework via 3d-to-2d queries," in *Proceedings of the IEEE/CVF Conference on Computer Vision and Pattern Recognition*, 2022, pp. 4537–4546.
- [14] A. Rasouli, I. Kotseruba, and J. K. Tsotsos, "Are they going to cross? a benchmark dataset and baseline for pedestrian crosswalk behavior," in *Proceedings of the IEEE International Conference on Computer Vision Workshops*, 2017, pp. 206–213.
- [15] A. Rasouli, I. Kotseruba, T. Kunic, and J. K. Tsotsos, "PIE: A large-scale dataset and models for pedestrian intention estimation and trajectory prediction," in *Proceedings of the IEEE/CVF International Conference on Computer Vision*, 2019, pp. 6262–6271.
- [16] B. Liu, E. Adeli, Z. Cao, K.-H. Lee, A. Sheno, A. Gaidon, and J. C. Niebles, "Spatiotemporal relationship reasoning for pedestrian intent prediction," *IEEE Robotics and Automation Letters*, vol. 5, no. 2, pp. 3485–3492, 2020.
- [17] I. Kotseruba, A. Rasouli, and J. K. Tsotsos, "Benchmark for evaluating pedestrian action prediction," in *Proceedings of the IEEE/CVF Winter Conference on Applications of Computer Vision*, 2021, pp. 1258–1268.
- [18] F. Schneemann and P. Heinemann, "Context-based detection of pedestrian crossing intention for autonomous driving in urban environments," in *2016 IEEE/RSJ International Conference on Intelligent Robots and Systems (IROS)*. IEEE, 2016, pp. 2243–2248.
- [19] J. Mei, A. Z. Zhu, X. Yan, H. Yan, S. Qiao, L.-C. Chen, and H. Kretzschmar, "Waymo open dataset: Panoramic video panoptic segmentation," in *European Conference on Computer Vision*. Springer, 2022, pp. 53–72.
- [20] J. Gesnouin, S. Pechberti, B. Stanculescu, and F. Moutarde, "Assessing cross-dataset generalization of pedestrian crossing predictors," in *2022 IEEE Intelligent Vehicles Symposium (IV)*. IEEE, 2022, pp. 419–426.
- [21] H. Razali, T. Mordan, and A. Alahi, "Pedestrian intention prediction: A convolutional bottom-up multi-task approach," *Transportation research part C: emerging technologies*, vol. 130, p. 103259, 2021.
- [22] K. Cho, B. Van Merriënboer, C. Gulcehre, D. Bahdanau, F. Bougares, H. Schwenk, and Y. Bengio, "Learning phrase representations using rnn encoder-decoder for statistical machine translation," in *Proceedings of the 2014 Conference on Empirical Methods in Natural Language Processing (EMNLP)*, 2014, pp. 1724–1734.
- [23] A. Rasouli, I. Kotseruba, and J. K. Tsotsos, "Pedestrian action anticipation using contextual feature fusion in stacked rnns," in *British Machine Vision Conference*, 2020.
- [24] A. Bhattacharyya, M. Fritz, and B. Schiele, "Long-term on-board prediction of people in traffic scenes under uncertainty," in *Proceedings of the IEEE Conference on Computer Vision and Pattern Recognition*, 2018, pp. 4194–4202.
- [25] I. Kotseruba, A. Rasouli, and J. K. Tsotsos, "Do they want to cross? understanding pedestrian intention for behavior prediction," in *2020 IEEE Intelligent Vehicles Symposium (IV)*. IEEE, 2020, pp. 1688–1693.
- [26] J. Lorenzo, I. Parra, F. Wirth, C. Stiller, D. F. Llorca, and M. A. Sotelo, "RNN-based pedestrian crossing prediction using activity and pose-related features," in *2020 IEEE Intelligent Vehicles Symposium (IV)*. IEEE, 2020, pp. 1801–1806.
- [27] A. Singh and U. Suddamalla, "Multi-input fusion for practical pedestrian intention prediction," in *Proceedings of the IEEE/CVF International Conference on Computer Vision*, 2021, pp. 2304–2311.
- [28] K. Saleh, M. Hossny, and S. Nahavandi, "Real-time intent prediction of pedestrians for autonomous ground vehicles via spatio-temporal densenet," in *2019 International Conference on Robotics and Automation (ICRA)*, 2019, pp. 9704–9710.
- [29] —, "Spatio-temporal densenet for real-time intent prediction of pedestrians in urban traffic environments," *Neurocomputing*, vol. 386, pp. 317–324, 2020.
- [30] J. Lorenzo, I. Parra, R. Izquierdo, A. L. Ballardini, Á. Hernández-Saz, D. F. Llorca, and M. A. Sotelo, "CAPformer: Pedestrian crossing action prediction using transformer," *Sensors (Basel, Switzerland)*, vol. 21, 2021.
- [31] S. Neogi, M. Hoy, K. Dang, H. Yu, and J. Dauwels, "Context model for pedestrian intention prediction using factored latent-dynamic conditional random fields," *IEEE transactions on intelligent transportation systems*, vol. 22, no. 11, pp. 6821–6832, 2020.
- [32] D. Zhang, F. Shi, Y. Meng, Y. Xu, X. Xiao, and W. Li, "Pedestrian intention prediction via depth augmented scene restoration," in *2021 5th CAA International Conference on Vehicular Control and Intelligence (CVCI)*. IEEE, 2021, pp. 1–6.
- [33] Z. Fang and A. M. López, "Is the pedestrian going to cross? answering by 2d pose estimation," in *2018 IEEE intelligent vehicles symposium (IV)*. IEEE, 2018, pp. 1271–1276.
- [34] Z. Fang and A. M. López, "Intention recognition of pedestrians and cyclists by 2d pose estimation," *IEEE Transactions on Intelligent Transportation Systems*, vol. 21, no. 11, pp. 4773–4783, 2020.
- [35] P. R. G. Cadena, Y. Qian, C. Wang, and M. Yang, "Pedestrian graph+: A fast pedestrian crossing prediction model based on graph convolutional networks," *IEEE Transactions on Intelligent Transportation Systems*, vol. 23, no. 11, pp. 21 050–21 061, 2022.
- [36] D. Yang, H. Zhang, E. Yurtsever, K. A. Redmill, and Ü. Özgüner, "Predicting pedestrian crossing intention with feature fusion and spatio-temporal attention," *IEEE Transactions on Intelligent Vehicles*, vol. 7, no. 2, pp. 221–230, 2022.
- [37] M. Azarmi, M. Rezaei, T. Hussain, and C. Qian, "Local and global contextual features fusion for pedestrian intention prediction," in *Artificial Intelligence and Smart Vehicles*, 2023, pp. 1–13.
- [38] H. Zhao, J. Jia, and V. Koltun, "Exploring self-attention for image recognition," in *Proceedings of the IEEE/CVF conference on computer vision and pattern recognition*, 2020, pp. 10 076–10 085.
- [39] M. Rezaei, M. Azarmi, and F. M. P. Mir, "3D-Net: Monocular 3D object recognition for traffic monitoring," *Expert Systems with Applications*, vol. 227, p. 120253, 2023.
- [40] D. Maji, S. Nagori, M. Mathew, and D. Poddar, "YOLO-Pose: Enhancing YOLO for multi person pose estimation using object keypoint similarity loss," in *Proceedings of the IEEE/CVF Conference on Computer Vision and Pattern Recognition*, 2022, pp. 2637–2646.
- [41] E. Ilg, N. Mayer, T. Saikia, M. Keuper, A. Dosovitskiy, and T. Brox, "FlowNet 2.0: Evolution of optical flow estimation with deep networks," in *Proceedings of the IEEE conference on computer vision and pattern recognition*, 2017, pp. 2462–2470.
- [42] Y. Zhou, H. Zhang, H. Lee, S. Sun, P. Li, Y. Zhu, B. Yoo, X. Qi, and J.-J. Han, "Slot-vps: Object-centric representation learning for video panoptic segmentation," in *Proceedings of the IEEE/CVF Conference on Computer Vision and Pattern Recognition*, 2022, pp. 3093–3103.
- [43] J. Watson, O. Mac Aodha, V. Prisacariu, G. Brostow, and M. Firman, "The temporal opportunist: Self-supervised multi-frame monocular depth," in *Proceedings of the IEEE/CVF Conference on Computer Vision and Pattern Recognition*, 2021, pp. 1164–1174.

VI. BIOGRAPHY

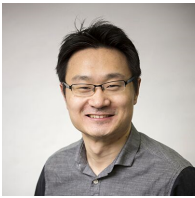


Mohsen Azarmi is a Ph.D. Student at the University of Leeds, Institute for Transport Studies, UK. He holds a master's degree in Artificial Intelligence & Robotics and his main research direction and expertise are Computer Vision, Deep Neural Networks, and multi-sensor data fusion with a particular focus on pedestrian activity recognition, transportation and traffic safety, and 3D scene modelling.



Mahdi Rezaei is an Associate Professor of Computer Science and ML and Leader of the Computer Vision Research Group at the University of Leeds, Institute for Transport Studies. He received his PhD in Computer Science from the University of Auckland, with the Top Thesis Award in 2014. Offering 18 years of service and research experience in academia and industry, Dr Rezaei has published 60+ journals and conference papers in top-tier venues. He is also the Principal Investigator and lead Co-Investigator of multiple European, UKRI,

and EPSRC AV-related projects such as L3Pilot, Hi-Drive, Research England, and MAVIS.



He Wang is an Associate Professor at the Department of Computer Science, University College London (UCL) and a Visiting Professor at the University of Leeds. He is the Director of High-Performance Graphics and Game Engineering and Academic Lead of Centre for Immersive Technology. His current research interest is mainly in computer graphics, vision and machine learning and applications.



Sebastien Glaser is a Professor of Intelligent Transportation Systems at the Center for Accident Research & Road Safety (CARS) at Queensland University of Technology, Australia. He received his Ph.D. in Automatic and Control (defining a driving assistance system in interaction with the driver) in 2004. He has worked in the development of Automated Driving Systems in interaction with other road users and